Sensor Sensitivity Based on Exceptional Points Engineered via Synthetic Magnetism

S.R. Mbokop Tchounda,[1,*] P. Djorwé,[2,3,†] S.G. Nana Engo,[1,‡] and B. Djafari-Rouhani[4,§]

[1] *Department of Physics, Faculty of Science, University of Yaounde I, P.O. Box 812, Yaounde, Cameroon*

[2] *Department of Physics, Faculty of Science, University of Ngaoundere, P.O. Box 454, Ngaoundere, Cameroon*

[3] *Stellenbosch Institute for Advanced Study, Wallenberg Research Centre at Stellenbosch University, Stellenbosch, 7600, South Africa*

[4] *Faculté des Sciences et Technologies, Institut d'Électronique, de Microélectronique et nanotechnologie, UMR CNRS 8520 Université de Lille, 59652 Villeneuve d'Ascq, France*

(Received 8 February 2023; revised 13 April 2023; accepted 4 May 2023; published 6 June 2023)

An efficient mass sensor based on exceptional points (EPs), engineered under a synthetic magnetism requirement, is proposed. The benchmark system consists of an electromechanical (optomechanical) system where an electric (optical) field is driving two mechanical resonators that are mechanically coupled through a phase-dependent phonon hopping. This phase induces a series of EPs once it matches the condition of $\pi/2(2n+1)$. For any perturbation of the system, the phase-matched condition is no longer satisfied, and this lifts the EP degeneracies, leading to a frequency splitting that scales as the square root of the perturbation strength, resulting in a giant sensitivity-factor enhancement. Owing to the set of EPs, our proposal allows a multiple-sensing scheme and performs better than its anti-*PT*-symmetric sensor counterpart. This work sheds light on platforms that can be used for mass-sensing purposes, opening up new opportunities in nanoparticle or pollutant detection and in water treatment.

DOI: 10.1103/PhysRevApplied.19.064016

I. INTRODUCTION

Sensing is one of the most-important technological applications of electromagnetism. Sensor applications impact our daily life, and these applications include viruses or nanoparticle-like mass detection [1], environmental pollution [2], temperature sensors [3], biosensors [4], and salinity detection and water treatment [5–7]. Owing to these practical applications of sensing, it is crucial to seek an increase in sensitivity. Much attention has been paid recently to exceptional points (EPs), which are non-Hermitian singularities where the eigenvalues and their corresponding eigenstates coalesce. This interest is due to the counterintuitive features and intriguing effects happening in the vicinity of EPs. Among them are stopping light [8], loss-induced suppression and revival of lasing, pump-induced lasing death, unidirectional invisibility [9], collective phenomena [10,11], and sensor sensitivity enhancement. The interest in non-Hermitian sensors lies in the topological feature at the EP that induces sensitivity enhancement resulting from the frequency splitting that exhibits a square-root dependency on a small perturbation [12]. This exceptional-point sensitivity has been investigated in different fields, including optics [13,14], plasmonics [15], electronics [16–19], mechanics [20], and optomechanics [21]. Experimental comparison between an optical sensor based on EPs and an optical sensor based on diabolic points (i.e., the conventional Hermitian degeneracy) was made in Refs. [14,15], while sensitivity enhancement at the higher-order EP was demonstrated in Ref. [13]. A practical electronics EP microsensor was successfully implemented on a rat skin [17], and a better wireless sensing response was recorded and compared with the conventional approach based on diabolic points. Despite the different aspects of these systems, what is common to them is the EP engineering approach, which for most of them requires an amplification mechanism (gain) that is detrimental for sensing at the quantum level. Therefore, engineering EPs without a gain requirement has become a crucial key to better sensing. To overcome this limitation, anti-parity-time (A*PT*) symmetry [22] and a synthetic magnetic field have been proposed to engineer EPs in passive systems. Different approaches to create an artificial magnetic field have been proposed for specific purposes, such as nonreciprocal and topological bosonic transport [23–26], heating-resistant ground-state cooling [27],

*rolande.mbokop@facsciences-uy1.cm
†djorwepp@gmail.com
‡serge.nana-engo@facsciences-uy1.cm
§bahram.djafari-rouhani@univ-lille.fr

and dark-mode-breaking-induced noise-tolerant entanglement [28].

In this work, we propose a sensitivity enhancement of a sensor based on EPs that is engineered via synthetic magnetism. Our benchmark system consists of two mechanical resonators mechanically coupled and driven by a common optical or electrical signal. This system supports a phase-dependent phonon-hopping interaction (e.g., a phase modulation of the mechanical coupling strength), which is introduced to create synthetic magnetic fields. In contrast to the aforementioned sensors, sensors based on synthetic magnetism do not require an amplification mechanism, which is usually a tricky task (gain engineering) in experiments. Besides the removal of the need for this amplification process, we show that sensors of this class perform better than the passive anti-*PT*-symmetric sensors. Therefore, the presented approach of sensing provides insights to increase sensitivity and opens up new opportunities for sensor applications.

This work is organized as follows. In Sec. II, the model and its dynamical equations up to the EP features are described. Section III is devoted to sensitivity based on the synthetic magnetism feature, and Sec. IV concludes the work.

II. MODELING AND DYNAMICAL EQUATIONS

Our benchmark system is an electromechanical system where two mechanically coupled mechanical resonators are driven by a common electric field generated by an *LC* oscillator, as shown in Fig. 1(a). The rate of mechanical coupling J_m between the two mechanical resonators is modulated through a phase θ, which is introduced to create synthetic magnetic fields [28]. The same circuit can be modeled in an optomechanical system [23], as shown in Fig. 1(b). In the rotating frame of the driving fields (ω_p), the Hamiltonian ($\hbar = 1$) describing this system is

$$H = H_{\rm OM} + H_{\rm int} + H_{\rm drive} + H_\kappa + H_\gamma, \tag{1}$$

where

$$H_{\rm OM} = -\Delta a^\dagger a + \sum_{j=1,2} \left(\omega_j b_j^\dagger b_j - g_j a^\dagger a (b_j^\dagger + b_j)\right), \tag{2}$$

$$H_{\rm int} = J_m (e^{i\theta} b_1^\dagger b_2 + e^{-i\theta} b_1 b_2^\dagger), \tag{3}$$

$$H_{\rm drive} = i\sqrt{\kappa}\alpha^{\rm in}(a^\dagger + a), \tag{4}$$

where $H_{\rm OM}$, $H_{\rm int}$, and $H_{\rm drive}$ are the optomechanical, phonon-hopping-interaction, and driving Hamiltonian, respectively. In Eq. (1), H_κ (H_γ) is the Hamiltonian capturing the optical (mechanical) dissipation. The variables a and b_j are the annihilation bosonic field operators describing the optical and mechanical resonators, respectively. The mechanical displacements x_j are connected

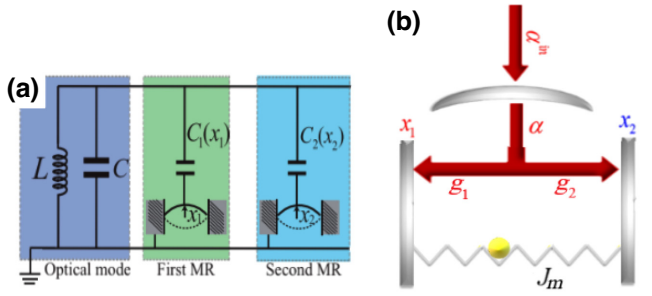

FIG. 1. (a) Electromechanical system where two mechanically coupled mechanical resonators (MRs) are driven by a common electric field from an *LC* oscillator. (b) An optomechanical equivalent system as in (a), where the yellow dot represents a small perturbation. The mechanical coupling rate J_m is dependent on the phase θ.

to the operators b_j as $x_j = x_{\rm ZPF}(b_j + b_j^\dagger)$, where $x_{\rm ZPF} = \sqrt{\hbar/2m\omega_j}$ is the zero-point-fluctuation amplitude of the mechanical resonator, with ω_j the mechanical frequency of the jth resonator. The frequency detuning between the driving (ω_p) and the cavity ($\omega_{\rm cav}$) is defined by $\Delta = \omega_p - \omega_{\rm cav}$. The driving strength is defined by $\alpha^{\rm in}$, and g_j is the optomechanical coupling. From the Heisenberg equation $\dot{\mathcal{O}} = i[H, \mathcal{O}] + \mathcal{N}$, where $\mathcal{O} \equiv (a, b_j)$ and $\mathcal{N} \equiv (a^{\rm in}, b_j^{\rm in})$ are the related noise operators, the quantum Langevin equations (QLEs) of our system read

$$\begin{aligned}
\dot{a} &= \left(i\left(\Delta - \sum_{j=1,2} g_j (b_j^\dagger + b_j)\right) - \frac{\kappa}{2}\right) a + \sqrt{\kappa}\alpha^{\rm in} + \sqrt{\kappa}a^{\rm in}, \\
\dot{b_1} &= -\left(i\omega_1 + \frac{\gamma_1}{2}\right) b_1 - iJ_m b_2 e^{i\theta} - ig_1 a^\dagger a + \sqrt{\gamma_1} b_1^{\rm in}, \\
\dot{b_2} &= -\left(i\omega_2 + \frac{\gamma_2}{2}\right) b_2 - iJ_m b_1 e^{-i\theta} - ig_2 a^\dagger a + \sqrt{\gamma_2} b_2^{\rm in}.
\end{aligned} \tag{5}$$

The noise operators $\mathcal{N} \equiv (a^{\rm in}, b_j^{\rm in})$ have zero mean and are characterized by the following autocorrelation functions [29]:

$$\langle \mathcal{N}(t)\mathcal{N}^\dagger(t')\rangle = (n_\nu + 1)\delta(t - t'), \tag{6}$$

$$\langle \mathcal{N}^\dagger(t)\mathcal{N}(t')\rangle = n_\nu \delta(t - t'), \tag{7}$$

with $n_\nu \equiv (n_{\rm th}, n_a)$, where $n_{\rm th} = \exp(\hbar\omega_j/k_B T - 1)^{-1}$ and $n_a = \langle a^{\rm in\dagger} a^{\rm in}\rangle$.

In this work, we are interested in the blue-sideband resonance, where $\Delta = \omega_m$, with $\omega_m = \omega_1$. The sensitivity performance of our proposed sensor is investigated by our computing the eigenvalues of the effective mechanical system, which allows us to identify the EP. To achieve that, we need to linearize the QLEs given in Eq. (5) and then integrate the optical field out of the resulting

system. The linearization process consists of splitting the field operators as $\mathcal{O} = \langle O \rangle + \delta\mathcal{O}$, where $\langle O \rangle$ is the coherent complex part of the operator and $\delta\mathcal{O}$ is its related fluctuation. The linearized dynamics (see Appendix A for details) can be treated by our moving to another interaction picture by introducing the following slowly varying operators with tildes: $\delta a = \delta\tilde{a}e^{i\tilde{\Delta}t}$ and $\delta b_j = \delta\tilde{b}_j e^{-i\omega_j t}$ where $\tilde{\Delta}$ is the effective detuning defined in Appendix A. In the limit of $\omega_j \gg (G_j, \kappa)$, with $G_j = g_j \langle a \rangle$, the rotating-wave approximation can be invoked, and we can obtain the following equation:

$$\delta\dot{\tilde{\mathcal{O}}} = -M\delta\tilde{\mathcal{O}} + \sqrt{K}\delta\tilde{\mathcal{N}}, \tag{8}$$

where the matrix M is given by

$$M = \begin{pmatrix} \frac{\kappa}{2} & iG_1 & iG_2 \\ iG_1^* & \frac{\gamma_1}{2} & iJ_m e^{i\theta} \\ iG_2^* & iJ_m e^{-i\theta} & \frac{\gamma_2}{2} \end{pmatrix} \tag{9}$$

and the noise coefficients are contained in the vector $K = (\kappa, \gamma_1, \gamma_2)^T$. Hereafter, and without loss of generality, we assume that the optomechanical coupling strengths G_1 and G_2 are positive real numbers and are set to be equal (i.e., $G_1 = G_2 = G$). Under the condition $\kappa \gg (G, \gamma_j)$, which is satisfied in our investigation, one can adiabatically eliminate the cavity field in Eq. (8), and this leads us to the effective dynamical system for the two mechanical resonators (see Appendix A for details):

$$i\partial_t \psi = H_{\text{eff}}\psi, \tag{10}$$

with $\psi = (\delta b_1, \delta b_2)$ and the effective Hamiltonian given by

$$H_{\text{eff}} = \begin{pmatrix} \omega_1 - \frac{i}{2}(\Gamma + \gamma_1) & J_m e^{i\theta} - i\frac{\Gamma}{2} \\ J_m e^{-i\theta} - i\frac{\Gamma}{2} & \omega_2 - \frac{i}{2}(\Gamma + \gamma_2) \end{pmatrix}, \tag{11}$$

where the optomechanical induced damping is defined as $\Gamma = 4G^2/\kappa$. The eigenvalues of the Hamiltonian given in Eq. (11) are

$$\lambda_\pm = \frac{1}{2}(\omega_1 + \omega_2) + \frac{i}{4}(\gamma_{\text{eff}}^1 + \gamma_{\text{eff}}^2) \pm \frac{\sigma}{4}, \tag{12}$$

where $\gamma_{\text{eff}}^j = \Gamma + \gamma_j$ and σ is defined as

$$\sigma = \sqrt{\chi - 16iJ_m\Gamma\cos\theta}, \tag{13}$$

with $\chi = (2\Delta\omega + i\Delta\gamma)^2 + 16J_m^2 - 4\Gamma^2$, where $\Delta\omega = \omega_1 - \omega_2$ and $\Delta\gamma = \gamma_{\text{eff}}^1 - \gamma_{\text{eff}}^2$. From these eigenvalues, the eigenfrequencies and eigendampings of the system are defined as being the real $[\omega_\pm = \text{Re}(\lambda_\pm)]$ and imaginary $\gamma_\pm = \text{Im}(\lambda_\pm)]$ parts of $\lambda_\pm$, respectively. At the EP, both these pairs of frequencies and dampings coalesce (i.e., $\omega_- = \omega_+$ and $\gamma_- = \gamma_+$), which means that $\sigma = 0$. This condition on σ can be fulfilled in our proposal by tuning of the driving field or the phase θ. For a proof of the concept of the proposed sensor based on synthetic magnetism EP engineering, we assume in the next section that the two mechanical resonators are slightly nondegenerate, allowing us to not be limited by the constraints related to the microfabrication variability.

III. SENSITIVITY ENHANCEMENT THROUGH SYNTHETIC MAGNETISM

The degree of the sensitivity of our sensor depends on the spectrum splitting at the EP once the system is perturbed. The perturbation can be a nanoparticule that has landed on the system or any mass deposition that is able to perturb the spectrum of the system. Therefore, we need to localize the EP before looking into our sensor feature. By assuming at first that $\gamma_1 = \gamma_2 = \gamma_m$ and that there is no direct coupling between the mechanical resonators ($J_m = 0$) for instance, we find σ reduces to

$$\sigma = 2\sqrt{\Delta\omega^2 - \Gamma^2}, \tag{14}$$

leading to an exceptional point at $\Gamma = \Delta\omega$, which is a result of an anti-*PT*-symmetric character of our system coming from the dissipative coupling induced by the cavity [27].

By turning on the phonon-hopping coupling ($J_m \neq 0$), we shift this EP to $\Gamma = \sqrt{\Delta\omega^2 + 4J_m^2}$ providing that $\theta = \pi/2(2n+1)$, with n being an integer. In Fig. 2, we depict the eigenfrequencies [Fig. 2(a)] and eigendamping [Fig. 2(b) of our system for $J_m \neq 0$, and they both coalesce at the EP. To show the θ dependence of the eigenvalues,

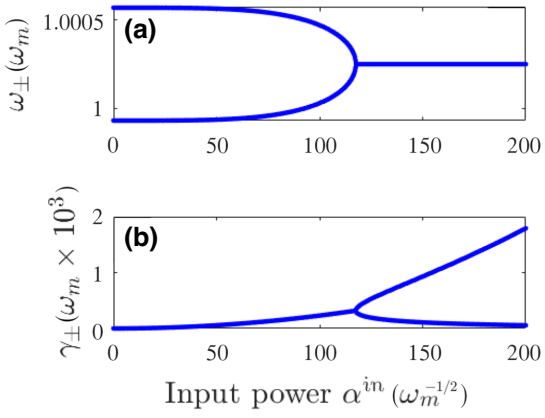

FIG. 2. (a) Eigenfrequencies and (b) eigendampings of the system in the presence of synthetic magnetism. The parameters used are $\omega_1 = \omega_m$, $\omega_2 = (1 + 5 \times 10^{-4})\omega_m$, $\kappa = 7.3 \times 10^{-2}\omega_m$, $\Delta = \omega_m$, $g = 1.077 \times 10^{-4}\omega_m$, $\gamma_1 = 1.077 \times 10^{-5}\omega_m$, $\gamma_2 = \gamma_1$, $J_m = 2 \times 10^{-4}\omega_m$, and $\theta = \pi/2$.

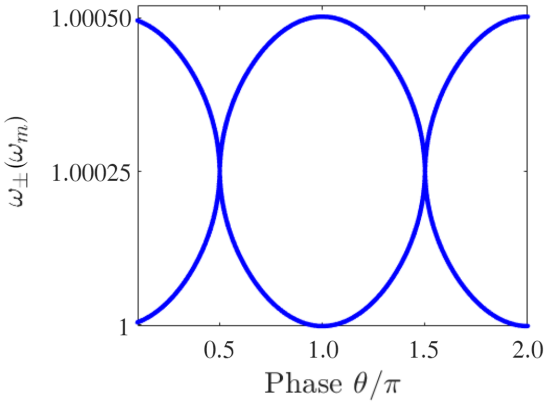

FIG. 3. Eigenfrequencies versus θ, where we can see the EPs engineered through the phase modulation at $\pi/2(2n+1)$. The parameters used are the same as for Fig. 2, and the driving-field amplitude corresponds to the EP ($\alpha^{\text{in}} \sim 117\omega_m^{1/2}$) shown in Fig. 2.

we sketch in Fig. 3 the eigenfrequencies versus the phase, and it can be seen that the EP occurs at $\theta = \pi/2(2n+1)$. To obtain insight into our sensor feature, we assume that a mass [see the yellow dot in Fig. 1(b), for instance] has been deposited on the system. This mass will act as a perturbation on our system that will lift the degeneracy at the EP, as shown in Fig. 4. Since our investigation is focused on the synthetic magnetism effect, we assume that this perturbation mainly induces a phase shift in our system. Indeed, it was shown in recent work that a magnetic field can be generated by the introduction of a frequency difference between the mechanical modes of an optomechanical crystal [23] or by a smooth geometry modification of a snowflake phononic crystal through a tiny perturbation [30]. These different schemes suggest the possibility to tune the phase of the synthetic magnetic field through weak perturbation as a mass deposition on the structure. Therefore, the perturbed-eigenvalue spectrum will depend on $\theta \pm \delta\theta$ instead, where $\delta\theta$ is the phase shift resulting from the perturbation. Such a perturbation leads to the splitting shown in Fig. 4(a), where the perturbation is introduced at the EP corresponding to $n = 0$ ($\theta = \pi/2$). The related sensitivity is captured in Fig. 4(b), where the highest splitting shown by the peak at the EP reveals the efficiency of our proposed sensor. Moreover, the same sensitivity can be determined when the EPs appearing for

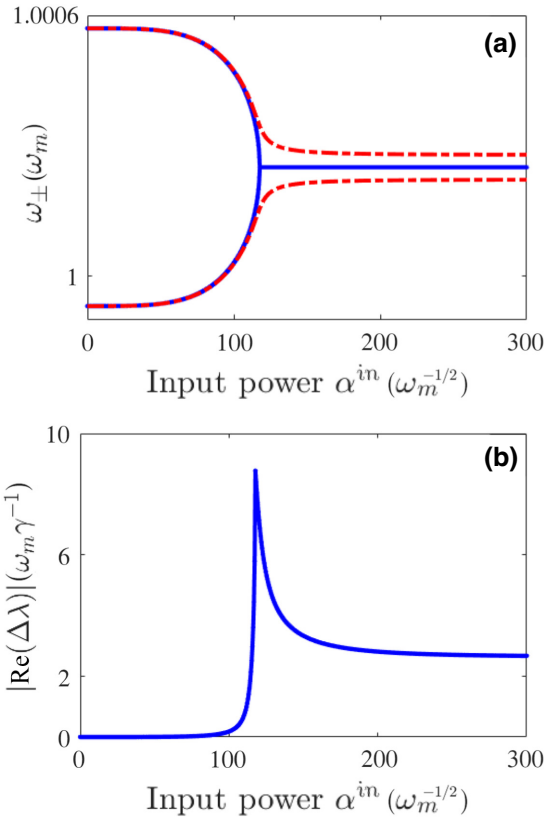

FIG. 4. (a) Eigenfrequency splitting and (b) the resulting splitting after a perturbation [see the dashed curve in (a)]. The parameters used are the same as for Fig. 2, and the perturbation strength $\epsilon = 0.2$.

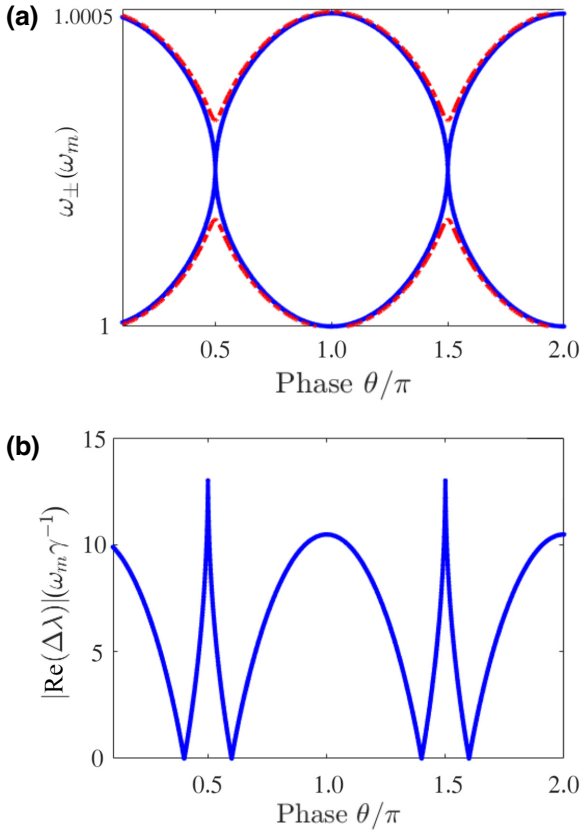

FIG. 5. (a) Eigenfrequencies versus θ and (b) the resulting splitting versus θ after a perturbation ($\epsilon = 0.5$). The parameters used are the same as for Fig. 2. The driving-field amplitude of the dashed curve in (a) is given by $\alpha^{\text{in}} = 115\omega_m^{1/2}$, and it shows how the EP can be lifted when the field amplitude is not well tuned. The possibility of multiple detection at the different EPs is shown in (b).

$n \neq 0$ are perturbed, as shown in Fig. 5, where Fig. 5(a) shows the splitting and Fig. 5(b) shows the related sensitivity. It can be seen that such a sensor can be used for detection at more than one EP, and such a feature may be interesting for a multiple-sensing scheme when several deposited masses have induced different perturbation strengths. For quantification purposes, a perturbation strength of ϵ acts on the phase as $\theta = \pi/(2 \pm \epsilon) \sim \pi/2(1 \pm \epsilon/2)$, which leads to the phase shift of $\delta\theta = \pm\epsilon\pi/4$. This phase shift acts on the eigenvalues given in Eq. (12) as

$$\lambda_{\pm}^{\delta\theta} = \frac{1}{2}(\omega_1 + \omega_2) + \frac{i}{4}(\gamma_{\text{eff}}^1 + \gamma_{\text{eff}}^2) \pm \frac{1}{4}\sqrt{\chi - 16iJ_m\Gamma(\cos\theta - \delta\theta\sin\theta)}. \quad (15)$$

We stress that this perturbation may also affect the optical dampings, but for the sake of a qualitative discussion and since the corresponding variations are very small, they are ignored in our analysis. To quantitatively give a meaning to the simulated results depicted in Figs. 4 and 5, we define the sensitivity as the absolute value of the frequency shift of an eigenfrequency from its reference signal; that is, $\text{Re}(\Delta\lambda_{\pm}) \equiv \text{Re}(\lambda_{\pm}^{\delta\theta} - \lambda_{\pm})$. Owing to the high sensitivity at the EP (see the high peaks in Figs. 4 and 5,) the related splitting of the eigenvalues can be expressed as (see Appendix B)

$$\Delta\lambda_{\pm}^{\text{EP}} = \pm\frac{(1+i)}{2}\sqrt{2\delta\theta J_m\Gamma}, \quad (16)$$

which shows that there is no splitting at the EP for $\delta\theta = 0$ as expected. Once the system is perturbed ($\delta\theta \neq 0$), Eq. (16) reveals that the eigenfrequencies experience the same splitting [$\text{Re}(\Delta\lambda_-) = \text{Re}(\Delta\lambda_+)$], as can be seen in Fig. 4. Another feature revealed from Eq. (16) is that the splitting at the EP scales as the square root of the strength of the perturbation (proportional to $\delta\theta^{1/2}$), in stark contrast with the linear dependence for conventional sensors [21]. Owing to this complex square-root topology, EP sensors perform better in detecting small mass deposition than conventional sensors, as can be seen in Fig. 6, where both the sensitivity and the enhancement factor are shown. The enhancement factor is defined from Eq. (16) as

$$\eta \equiv \left|\frac{\text{Re}(\Delta\lambda^{\text{EP}})}{\delta\theta}\right| = \sqrt{\frac{J_m\Gamma}{2\delta\theta}}. \quad (17)$$

For comparison purposes, we consider two other cases where the phase θ is not perturbed. The first one is the anti-*PT*-symmetric sensor case ($J_m = 0$), where the perturbation will induce a change in the resonator quality factor ($Q_j = \omega_j/\gamma_j$) rather than in the phase. The second case is when the two mechanical resonators are coupled ($J_m \neq 0$), but the splitting is likewise induced by the quality-factor perturbation. These two cases together with the phase-shift perturbation are compared in Fig. 6 for the sensitivity and the enhancement factor, respectively. In Fig. 6(a), a great increase in the sensitivity can be seen when the phase is perturbed (full curve) as compared with the cases where the quality factor (the damping rate, for instance) is perturbed. Moreover, regarding the cases where the quality factor is perturbed (dash-dotted and dashed curves), Fig. 6(a) reveals that the anti-*PT*-symmetric sensor (dash-dotted curve) has less sensitivity than the sensor operating at the EP engineered without a synthetic magnetism condition (dashed curve). This feature reveals that phase perturbation has a profound impact on our sensor, which in turn indicates the sensing efficiency when the sensor is operating under the synthetic magnetism requirement. This sensing scheme based on an EP, which does not require gain, offers new opportunities to enhance sensing. Furthermore, Fig. 6(b) shows the enhancement factor versus the perturbation strength. A giant sensing enhancement under the phase-perturbation approach, as mentioned for

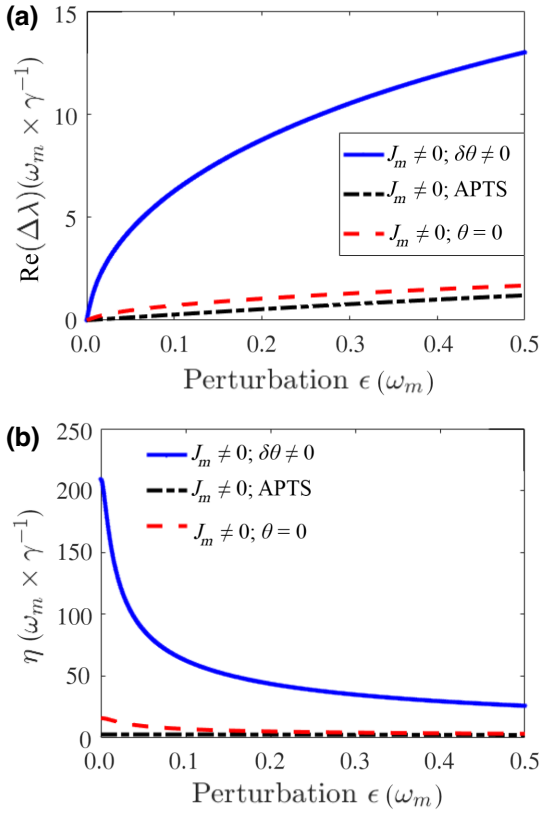

FIG. 6. (a) Sensitivity at the exceptional point versus the strength of the perturbation ϵ. (b) Enhancement factor η versus ϵ. It can be seen that for weak perturbation our proposed sensor performs better, and this performance decreases as the perturbation increases. Also, the sensor under synthetic magnetism is more efficient than the two other cases [see the dashed and dash-dotted curves in (a) and (b)]. APTS, anti-parity-time symmetry.

Fig. 6(a), can be seen. As the strength of the perturbation increases, the enhancement factor η decreases. For strong-enough perturbation, η evolves toward a limit bounded by the other two cases, where the quality factor is perturbed. More importantly, the η behavior shows how well our sensor performs for weak perturbation strength, proving the efficiency of the EP sensor in detecting small particles and diverse pollutants.

IV. CONCLUSION

We investigate sensor sensitivity based on exceptional points engineered under a synthetic magnetism requirement. One advantage of this approach is that we can operate without the requirement of gain, which substantially makes experimental tasks easier. Our system can be thought of as an electromechanical (optomechanical) system where an electric (optical) field is driving two mechanical resonators that are mechanically coupled through a phase-dependent phonon-hopping rate. We show that this phase induces a series of EPs, which occur at the phase-matched condition of $\pi/2(2n+1)$. When there is no direct coupling between the two mechanical resonators, our system still hosts an EP owing to an anti-*PT*-symmetry feature coming form the dissipative coupling induced by the cavity. For that reason, two perturbation schemes are considered in our investigation, one related to the quality factor and the other acting on the phase dependence. Our study shows that the sensor performs better when the phase is perturbed rather than the quality factor. Moreover, this approach involving synthetic magnetism allows a multiple-sensing scheme owing to the series of phase-induced exceptional points in the system. This work provides opportunities for sensitivity enhancement and sheds light on platforms that can be used to develop efficient sensors.

ACKNOWLEDGMENTS

This work was conducted under the Iso-Lomso Fellowship at the Stellenbosch Institute for Advanced Study, Wallenberg Research Centre at Stellenbosch University, Stellenbosch, South Africa. P.D. and S.G.N.E. thank the Ministry of Higher Education of Cameroon (MINESUP) for financial assistance within the framework of the "Research Modernization" allowances.

APPENDIX A: EFFECTIVE HAMILTONIAN

Here we provide details of the dynamical equations from the QLEs [see Eq. (5)] to the effective Hamiltonian given in Eq. (11). Starting with the QLEs, we linearize our system by splitting the bosonic operators a and b into their average part plus an amount of fluctuation as $a = \alpha + \delta a$ and $b_j = \beta_j + \delta b_j$, with $\alpha = \langle a \rangle$ and $\beta_j = \langle b_j \rangle$. The linearization process leads to the averaged dynamics,

$$\begin{aligned}
\dot{\alpha} &= \left(i\tilde{\Delta} - \frac{\kappa}{2}\right)\alpha + \sqrt{\kappa}\alpha^{\text{in}}, \\
\dot{\beta_1} &= -\left(i\omega_1 + \frac{\gamma_1}{2}\right)\beta_1 - iJ_m e^{i\theta}\beta_2 - ig_1|\alpha|^2, \\
\dot{\beta_2} &= -\left(i\omega_2 + \frac{\gamma_2}{2}\right)\beta_2 - iJ_m e^{-i\theta}\beta_1 - ig_2|\alpha|^2,
\end{aligned} \tag{A1}$$

and to the fluctuation dynamics,

$$\begin{aligned}
\delta\dot{a} &= \left(i\tilde{\Delta} - \frac{\kappa}{2}\right)\delta a - i\sum_j g_j(\delta b_j^\dagger + \delta b_j)\alpha + \sqrt{\kappa}a^{\text{in}}, \\
\delta\dot{b_1} &= -\left(i\omega_1 + \frac{\gamma_1}{2}\right)\delta b_1 - iJ_m e^{i\theta}\delta b_2 - ig_1(\alpha^\dagger\delta a + \alpha\delta a^\dagger) + \sqrt{\gamma_1}b_1^{\text{in}}, \\
\delta\dot{b_2} &= -\left(i\omega_2 + \frac{\gamma_2}{2}\right)\delta b_2 - iJ_m e^{-i\theta}\delta b_1 - ig_2(\alpha^\dagger\delta a + \alpha\delta a^\dagger) + \sqrt{\gamma_2}b_2^{\text{in}},
\end{aligned} \tag{A2}$$

where the effective detuning is defined as $\tilde{\Delta} = \Delta - 2\sum_j g_j \text{Re}(\beta_j)$. The stability of our system can be studied with the set of equations in Eq. (A1), while the dynamical fluctuation captured by the set of equations in Eq. (A2) describes the behavior of our system in the linearized regime. It can be treated by introducing the following slowly varying operators with tildes, $\delta a = \delta\tilde{a}e^{i\tilde{\Delta}t}$ and $\delta b_j = \delta\tilde{b_j}e^{-i\omega_j t}$. This results in the following set of equations:

$$\begin{aligned}
\delta\dot{\tilde{a}} &= -\frac{\kappa}{2}\delta\tilde{a} - i\sum_j G_j(\delta\tilde{b_j}^\dagger e^{i(\omega_j-\tilde{\Delta})t} + \delta\tilde{b_j}e^{-i(\omega_j+\tilde{\Delta})t}) + \sqrt{\kappa}\tilde{a}^{\text{in}}, \\
\delta\dot{\tilde{b_1}} &= -\frac{\gamma_1}{2}\delta\tilde{b_1} - iJ_m\delta\tilde{b_2}e^{i\theta}e^{-i(\omega_2-\omega_1)t} - ig_1(\alpha^\dagger\delta\tilde{a}e^{i(\tilde{\Delta}+\omega_1)t} + \alpha\delta\tilde{a}^\dagger e^{-i(\tilde{\Delta}-\omega_1)t}) + \sqrt{\gamma_1}\tilde{b_1}^{\text{in}}, \\
\delta\dot{\tilde{b_2}} &= -\frac{\gamma_2}{2}\delta\tilde{b_2} - iJ_m\delta\tilde{b_1}e^{-i\theta}e^{-i(\omega_1-\omega_2)t} - ig_2(\alpha^\dagger\delta\tilde{a}e^{i(\tilde{\Delta}+\omega_2)t} + \alpha\delta\tilde{a}^\dagger e^{-i(\tilde{\Delta}-\omega_2)t}) + \sqrt{\gamma_2}\tilde{b_2}^{\text{in}}.
\end{aligned} \tag{A3}$$

For simplicity, we focus our attention during this investigation on the blue-sideband resonance $\tilde{\Delta} = \omega_j$. Under this assumption, the set of equations in Eq. (A3) reduces to

$$\begin{aligned}
\delta\dot{\tilde{a}} &= -\frac{\kappa}{2}\delta\tilde{a} - i\sum_j G_j(\delta\tilde{b_j}^{\dagger}e^{2i\omega_j t} + \delta\tilde{b_j}) + \sqrt{\kappa}\tilde{a}^{\text{in}},\\
\delta\dot{\tilde{b_1}} &= -\frac{\gamma_1}{2}\delta\tilde{b_1} - iJ_m\delta\tilde{b_2}e^{i\theta} - ig_1(\alpha^{\dagger}\delta\tilde{a} + \alpha\delta\tilde{a}^{\dagger}e^{-2i\tilde{\Delta}t}) + \sqrt{\gamma_1}\tilde{b_1}^{\text{in}},\\
\delta\dot{\tilde{b_2}} &= -\frac{\gamma_2}{2}\delta\tilde{b_2} - iJ_m\delta\tilde{b_1}e^{-i\theta} - ig_2(\alpha^{\dagger}\delta\tilde{a} + \alpha\delta\tilde{a}^{\dagger}e^{-2i\tilde{\Delta}t}) + \sqrt{\gamma_2}\tilde{b_2}^{\text{in}}.
\end{aligned} \tag{A4}$$

Under the limit of $\omega_j \gg (G_j, \kappa)$, we can invoke the rotating-wave approximation by dropping the fast-rotating terms, and the set of equations in Eq. (A4) further simplifies to

$$\begin{aligned}
\delta\dot{\tilde{a}} &= -\frac{\kappa}{2}\delta\tilde{a} - i\sum_j G_j\,\delta\tilde{b_j}) + \sqrt{\kappa}\tilde{a}^{\text{in}},\\
\delta\dot{\tilde{b_1}} &= -\frac{\gamma_1}{2}\delta\tilde{b_1} - iJ_m\delta\tilde{b_2}e^{i\theta} - iG_1^{*}\delta\tilde{a} + \sqrt{\gamma_1}\tilde{b_1}^{\text{in}},\\
\delta\dot{\tilde{b_2}} &= -\frac{\gamma_2}{2}\delta\tilde{b_2} - iJ_m\delta\tilde{b_1}e^{-i\theta} - iG_2^{*}\delta\tilde{a} + \sqrt{\gamma_2}\tilde{b_2}^{\text{in}},
\end{aligned} \tag{A5}$$

which is given in its compact form by Eq. (8). Under the hierarchy of parameters $\kappa \gg (G, \gamma_j)$, which is fulfilled here, we can adiabatically eliminate the cavity field in Eq. (A5) to get the mechanical effective system revealed through Eq. (10).

APPENDIX B: PERTURBED EIGENVALUES AND SENSITIVITY

The phase perturbation of the eigenvalues given by Eq. (15) is explicitly written as

$$\lambda_{\pm}^{\delta\theta} = \xi \pm \frac{1}{4}\sqrt{\chi - 16iJ_m\Gamma\cos(\theta + \delta\theta)}, \tag{B1}$$

where we set

$$\xi = \frac{1}{2}(\omega_1 + \omega_2) + \frac{i}{4}(\gamma_{\text{eff}}^1 + \gamma_{\text{eff}}^2), \tag{B2}$$

and

$$\chi = (2\Delta\omega + i\Delta\gamma)^2 + 16J_m^2 - 4\Gamma^2. \tag{B3}$$

As the perturbation $\delta\theta$ is small, one can assume that

$$\begin{aligned}
\cos(\theta + \delta\theta) &= \cos(\theta)\cos(\delta\theta) - \sin(\theta)\sin(\delta\theta)\\
&\sim \cos(\theta) - \delta\theta\sin(\theta),
\end{aligned} \tag{B4}$$

which leads to

$$\lambda_{\pm}^{\delta\theta} = \xi \pm \frac{1}{4}\sqrt{\sigma^2 + 16iJ_m\Gamma\delta\theta\sin(\theta)}. \tag{B5}$$

The sensitivity of our system is evaluated as the difference between the perturbed and the nonperturbed spectra (i.e., $\Delta\lambda = \lambda_{\pm}^{\delta\theta} - \lambda_{\pm}$) as

$$\begin{aligned}
\Delta\lambda = \lambda_{\pm}^{\delta\theta} - \lambda_{\pm} &= \xi \pm \frac{1}{4}\sqrt{\sigma^2 + 16iJ_m\Gamma\delta\theta\sin(\theta)}\\
&\quad - \left(\xi \pm \frac{\sigma}{4}\right)\\
&= \pm\frac{1}{4}\sqrt{\sigma^2 + 16iJ_m\Gamma\delta\theta\sin(\theta)} \mp \frac{\sigma}{4}.
\end{aligned} \tag{B6}$$

As we seek to evaluate this sensitivity at the EP, this means that the following requirements have to be considered: $\theta = \pi/2$ and $\sigma = 0$. Therefore, the overall splitting at the EP yields

$$\Delta\lambda_{\pm}^{\text{EP}} = \pm\sqrt{i\delta\theta J_m\Gamma}. \tag{B7}$$

By using $\sqrt{i} = \sqrt{2}/2(1 + i)$, we can express Eq. (B7) in the form,

$$\Delta\lambda_{\pm}^{\text{EP}} = \pm\frac{\sqrt{2}}{2}(1 + i)\sqrt{\delta\theta J_m\Gamma}, \tag{B8}$$

which clearly shows the square-root dependence to the perturbation $\delta\theta$ as expected. As the sensitivity is defined as $\text{Re}(\Delta\lambda^{\text{EP}})$, one finally deduces that

$$\Delta\omega_{\pm}^{\text{EP}} = \text{Re}(\Delta\lambda_{\pm}^{\text{EP}}) = \pm\frac{\sqrt{2}}{2}\sqrt{\delta\theta J_m\Gamma}. \tag{B9}$$

In the two other cases, shown by the dashed and dash-dotted curves in Fig. 6, the sensitivity is not given by Eq. (B9). Because $\theta = 0$ in these cases, the perturbation is instead introduced through the quality factor. By assuming a perturbation ϵ induces a dissipation shift of strength $\delta\gamma$, we can quantify the perturbed eigenvalues as

$$\lambda_{\pm}^{\delta\gamma} = \xi + \frac{i\delta\gamma}{4} \pm \frac{1}{4}\sqrt{\chi^{\delta\gamma} - 16iJ_m\Gamma\cos\theta}, \tag{B10}$$

where

$$\chi^{\delta\gamma} = (2\Delta\omega + i(\Delta\gamma + \delta\gamma))^2 + 16J_m^2 - 4\Gamma^2. \tag{B11}$$

The corresponding splitting is then $\Delta\lambda = \lambda_{\pm}^{\delta\gamma} - \lambda_{\pm}$ as

$$\Delta\lambda = \xi + \frac{i\delta\gamma}{4} \pm \frac{1}{4}\sqrt{\sigma^2 + 4i\delta\gamma\Delta\omega - \delta\gamma^2} - \left(\xi \pm \frac{\sigma}{4}\right)$$
$$= \frac{i\delta\gamma}{4} \pm \frac{1}{4}\sqrt{\sigma^2 + 4i\delta\gamma\Delta\omega - \delta\gamma^2} \mp \frac{\sigma}{4}. \quad \text{(B12)}$$

At the EP, this sensitivity leads to

$$\Delta\lambda = \frac{i\delta\gamma}{4} \pm \frac{1}{4}\sqrt{4i\delta\gamma\Delta\omega - \delta\gamma^2}. \quad \text{(B13)}$$

From Eq. (B13), it can be seen that without perturbation ($\delta\gamma = 0$), there is no splitting at the EP as expected. Moreover, as the perturbation is usually small ($\delta\gamma^2 \sim 0$), Eq. (B13) can be expressed as

$$\Delta\lambda \sim \frac{1}{4}\left(i(\delta\gamma \pm \sqrt{2\delta\gamma\Delta\omega}) \pm \sqrt{2\delta\gamma\Delta\omega}\right). \quad \text{(B14)}$$

The related sensitivity, which is the real part, can be deduced as

$$\Delta\omega_{\pm}^{\mathrm{EP}} = \mathrm{Re}(\Delta\lambda_{\pm}^{\mathrm{EP}}) \sim \pm\frac{1}{2}\sqrt{\frac{\delta\gamma\Delta\omega}{2}}, \quad \text{(B15)}$$

with scales as $\delta\gamma^{1/2}$ as expected as well. From the definition of the enhancement factor, we obtain

$$\eta = \frac{\Delta\omega_{\pm}^{\mathrm{EP}}}{\delta\gamma} = \pm\frac{1}{2}\sqrt{\frac{\Delta\omega}{2\delta\gamma}}. \quad \text{(B16)}$$

[1] S. Marquez, M. Alvarez, J. A. Plaza, L. G. Villanueva, C. Dominguez, and L. M. Lechuga, Asymmetrically coupled resonators for mass sensing, Appl. Phys. Lett. **111**, 113101 (2017).

[2] Ashour M. Ahmed, Ahmed Mehaney, and Hussein A. Elsayed, Detection of toluene traces in exhaled breath by using a 1D PC as a biomarker for lung cancer diagnosis, Eur. Phys. J. Plus **136**, 626 (2021).

[3] Mansour Zaremanesh, Laurent Carpentier, Hamed Gharibi, Ali Bahrami, Ahmed Mehaney, Abdellatif Gueddida, Ralf Lucklum, Bahram Djafari-Rouhani, and Yan Pennec, Temperature biosensor based on triangular lattice phononic crystals, APL Mater. **9**, 061114 (2021).

[4] Ilyasse Quotane, Madiha Amrani, Cecile Ghouila-Houri, El Houssaine El Boudouti, Leonid Krutyansky, Bogdan Piwakowski, Philippe Pernod, Abdelkrim Talbi, and Bahram Djafari-Rouhani, A biosensor based on bound states in the continuum and Fano resonances in a solid liquid solid triple layer, Crystals **12**, 707 (2022).

[5] Iraj S. Amiri, Bikash Kumar Paul, Kawsar Ahmed, Arafa H. Aly, Rozalina Zakaria, Preecha Yupapin, and Dhasarathan Vigneswaran, Tri-core photonic crystal fiber based refractive index dual sensor for salinity and temperature detection, Microw. Opt. Technol. Lett. **61**, 847 (2018).

[6] Ralf Lucklum, Nikolay Mukhin, Bahram Djafari Rouhani, and Yan Pennec, Phononic crystal sensors: A new class of resonant sensors—chances and challenges for the determination of liquid properties, Front. Mech. Eng. **7**, 705194 (2021).

[7] R. Lucklum and J. Li, Phononic crystals for liquid sensor applications, Meas. Sci. Technol. **20**, 124014 (2009).

[8] Tamar Goldzak, Alexei A. Mailybaev, and Nimrod Moiseyev, Light Stops at Exceptional Points, Phys. Rev. Lett. **120**, 013901 (2018).

[9] B. Peng, Ş. K. Özdemir, S. Rotter, H. Yilmaz, M. Liertzer, F. Monifi, C. M. Bender, F. Nori, and L. Yang, Loss-induced suppression and revival of lasing, Science **346**, 328 (2014).

[10] P. Djorwe, Y. Pennec, and B. Djafari-Rouhani, Frequency locking and controllable chaos through exceptional points in optomechanics, Phys. Rev. E **98**, 032201 (2018).

[11] P. Djorwe, J. Y. Effa, and S. G. Nana Engo, Multistability, staircases, and optical high-order sideband combs in optomechanics, J. Opt. Soc. Am. A **37**, A36 (2020).

[12] Mohammad-Ali Miri and Andrea Alù, Exceptional points in optics and photonics, Science **363**, eaar7709 (2019).

[13] Hossein Hodaei, Absar U. Hassan, Steffen Wittek, Hipolito Garcia-Gracia, Ramy El-Ganainy, Demetrios N. Christodoulides, and Mercedeh Khajavikhan, Enhanced sensitivity at higher-order exceptional points, Nature **548**, 187 (2017).

[14] Weijian Chen, Şahin Kaya Özdemir, Guangming Zhao, Jan Wiersig, and Lan Yang, Exceptional points enhance sensing in an optical microcavity, Nature **548**, 192 (2017).

[15] Jun-Hee Park, Abdoulaye Ndao, Wei Cai, Liyi Hsu, Ashok Kodigala, Thomas Lepetit, Yu-Hwa Lo, and Boubacar Kanté, Symmetry-breaking-induced plasmonic exceptional points and nanoscale sensing, Nat. Phys. **16**, 462 (2020).

[16] Mingzhao Song, Prasad Jayathurathnage, Esmaeel Zanganeh, Mariia Krasikova, Pavel Smirnov, Pavel Belov, Polina Kapitanova, Constantin Simovski, Sergei Tretyakov, and Alex Krasnok, Wireless power transfer based on novel physical concepts, Nat. Electron. **4**, 707 (2021).

[17] Zhenya Dong, Zhipeng Li, Fengyuan Yang, Cheng-Wei Qiu, and John S. Ho, Sensitive readout of implantable microsensors using a wireless system locked to an exceptional point, Nat. Electron. **2**, 335 (2019).

[18] Weidong Cao, Changqing Wang, Weijian Chen, Song Hu, Hua Wang, Lan Yang, and Xuan Zhang, Fully integrated parity—time-symmetric electronics, Nat. Nanotechnol. **17**, 262 (2022).

[19] Pai-Yen Chen and Ramy El-Ganainy, Exceptional points enhance wireless readout, Nat. Electron. **2**, 323 (2019).

[20] Matheus I. N. Rosa, Matteo Mazzotti, and Massimo Ruzzene, Exceptional points and enhanced sensitivity in PT-symmetric continuous elastic media, J. Mech. Phys. Solids **149**, 104325 (2021).

[21] P. Djorwe, Y. Pennec, and B. Djafari-Rouhani, Low-power phonon lasing through position-modulated Kerr-type nonlinearity, Sci. Rep. **9**, 1684 (2019).

[22] Wenxiu Li, Hao Zhang, Peng Han, Xiaoyang Chang, Shuo Jiang, Yang Zhou, Anping Huang, and Zhisong Xiao, Real frequency splitting indirectly coupled anti-parity-time symmetric nanoparticle sensor, J. Appl. Phys. **128**, 134503 (2020).

[23] John P. Mathew, Javier del Pino, and Ewold Verhagen, Synthetic gauge fields for phonon transport in a nano-optomechanical system, Nat. Nanotechnol. **15**, 198 (2020).

[24] Kejie Fang, Zongfu Yu, and Shanhui Fan, Realizing effective magnetic field for photons by controlling the phase of dynamic modulation, Nat. Photonics. **6**, 782 (2012).

[25] Kejie Fang, Jie Luo, Anja Metelmann, Matthew H. Matheny, Florian Marquardt, Aashish A. Clerk, and Oskar Painter, Generalized non-reciprocity in an optomechanical circuit via synthetic magnetism and reservoir engineering, Nat. Phys. **13**, 465 (2017).

[26] M. Schmidt, S. Kessler, V. Peano, O. Painter, and F. Marquardt, Optomechanical creation of magnetic fields for photons on a lattice, Optica **2**, 635 (2015).

[27] Cheng Jiang, Yu-Long Liu, and Mika A. Sillanpää, Energy-level attraction and heating-resistant cooling of mechanical resonators with exceptional points, Phys. Rev. A. **104**, 013502 (2021).

[28] Deng-Gao Lai, Jie-Qiao Liao, Adam Miranowicz, and Franco Nori, Noise-Tolerant Optomechanical Entanglement via Synthetic Magnetism, Phys. Rev. Lett. **129**, 063602 (2022).

[29] C. Tchodimou, P. Djorwe, and S. G. Nana Engo, Distant entanglement enhanced in PT-symmetric optomechanics, Phys. Rev. A **96**, 033856 (2017).

[30] Christian Brendel, Vittorio Peano, Oskar J. Painter, and Florian Marquardt, Pseudomagnetic fields for sound at the nanoscale, Proc. Natl. Acad. Sci. **114**, E3390 (2017).